Systematic identification of pathological lamin A interactors

Travis A. Dittmer[a], Nidhi Sahni[b,c], Nard Kubben[a], David E. Hill[b,c], Marc Vidal[b,c], Rebecca C. Burgess[a], Vassilis Roukos[a], and Tom Misteli[a]

[a]National Cancer Institute, National Institutes of Health, Bethesda, MD 20892; [b]Center for Cancer Systems Biology and Department of Cancer Biology, Dana-Farber Cancer Institute, Boston, MA 02215; [c]Department of Genetics, Harvard Medical School, Boston, MA 02215

ABSTRACT **Laminopathies are a collection of phenotypically diverse diseases that include muscular dystrophies, cardiomyopathies, lipodystrophies, and premature aging syndromes. Laminopathies are caused by >300 distinct mutations in the *LMNA* gene, which encodes the nuclear intermediate filament proteins lamin A and C, two major architectural elements of the mammalian cell nucleus. The genotype–phenotype relationship and the basis for the pronounced tissue specificity of laminopathies are poorly understood. Here we seek to identify on a global scale lamin A–binding partners whose interaction is affected by disease-relevant *LMNA* mutations. In a screen of a human genome–wide ORFeome library, we identified and validated 337 lamin A–binding proteins. Testing them against 89 known lamin A disease mutations identified 50 disease-associated interactors. Association of progerin, the lamin A isoform responsible for the premature aging disorder Hutchinson–Gilford progeria syndrome, with its partners was largely mediated by farnesylation. Mapping of the interaction sites on lamin A identified the immunoglobulin G (IgG)–like domain as an interaction hotspot and demonstrated that lamin A variants, which destabilize the Ig-like domain, affect protein–protein interactions more globally than mutations of surface residues. Analysis of a set of LMNA mutations in a single residue, which result in three phenotypically distinct diseases, identified disease-specific interactors. The results represent a systematic map of disease-relevant lamin A interactors and suggest loss of tissue-specific lamin A interactions as a mechanism for the tissue-specific appearance of laminopathic phenotypes.**

Monitoring Editor
Martin Hetzer
Salk Institute for Biological Studies

Received: Feb 10, 2014
Revised: Mar 3, 2014
Accepted: Mar 4, 2014

This article was published online ahead of print in MBoC in Press (http://www.molbiolcell.org/cgi/doi/10.1091/mbc.E14-02-0733) on March 12, 2014.

Address correspondence to: Tom Misteli (mistelit@mail.nih.gov).

Abbreviations used: AD, activation domain; 3-AT, 3-amino-1, 2, 4-triazole; BP, biological process; CC, cellular components; CHX, cycloheximide; CMD1A, cardiomyopathy; CMT2B1, Charcot-Marie-Tooth neuropathy; cyto, cytoplasmic; DB, DNA-binding domain; EDMD, Emery-Dreifuss muscular dystrophy; ER, endoplasmic reticulum; FPLD, Dunnigan-type familiar partial lipodystrophy; GO, Gene Ontology; HPGS, Hutchinson-Gilford progeria syndrome; Ig, immunoglobulin; LAF, lone atrial fibrillation; LGMD1B, limb girdle muscular dystrophy; MADA, mandibuloacral dysplasia with type A lipodystrophy; MF, molecular function; NE, nuclear envelope; NLS, nuclear localization signal; nuc, nuclear; ORF, open reading frame; OST, OneStrepTag; RD, restrictive dermopathy; RSS, lamin-related rigid spine muscular dystrophy; YFP, yellow fluorescent protein; Y2H, yeast two hybrid.

INTRODUCTION

The nuclear envelope (NE) defines the boundary between the nucleus and the cytoplasm (Macara, 2001; Dittmer and Misteli, 2011). The nucleoplasmic face of the NE is lined by the nuclear lamina, a dense protein interface connecting the inner nuclear membrane and chromatin (Stuurman *et al*., 1998; Dittmer and Misteli, 2011). Major structural constituents of the lamina are the intermediate filament proteins lamins A and C, encoded by the *LMNA* gene (Fisher *et al*., 1986). The A-type lamins are ubiquitously expressed in most adult somatic cells and assemble into higher-order filaments. Together with the B-type lamins, expressed from separate genes, lamin complexes contribute to nuclear structure and influence nuclear organization (Dittmer and Misteli, 2011).

Although the most-studied functional aspects of A-type lamins are the structural roles they play during interphase, lamins A/C are increasingly recognized as mediators, and possibly regulators, of

diverse nuclear processes (Gonzalez *et al.*, 2011). They are implicated in higher-order genome organization, since they physically interact with chromatin, and cells deficient for lamins A/C show a loss of peripheral heterochromatin, ectopic chromatin condensation, and mispositioning of centromeric heterochromatin (Taniura *et al.*, 1995; Sullivan *et al.*, 1999; Nikolova *et al.*, 2004; Galiova *et al.*, 2008; Bruston *et al.*, 2010). Lamins A/C may also play a role in DNA repair as cells expressing mutant forms of lamin A exhibit a delay in recruitment of repair factors to sites of DNA damage and show increased levels of double-strand breaks (Liu *et al.*, 2005; Manju *et al.*, 2006). Lamins A/C have also been linked to signal transduction pathways involved in differentiation and homeostasis by regulating the activity and availability of proteins within the mitogen-activated protein kinase– and RB-cell cycle pathways (Gonzalez *et al.*, 2011). They are also implicated in transcription and DNA replication, possibly by aiding assembly of the transcription and replication machineries (Kumaran *et al.*, 2002; Spann *et al.*, 2002; Zastrow *et al.*, 2004).

Many of these activities rely on lamin A/C–protein interactions. Lamins A/C associate with B-type lamins and homopolymerize (Ye and Worman, 1995). In addition to lamin–lamin interactions, lamins bind to proteins anchored in the inner nuclear membrane, such as thymopoietin (TMPO; LAP2) or emerin (Zastrow *et al.*, 2004). Together with SUN1 and nesprins, lamins form the LINC (linkers of the nucleoskeleton to the cytoskeleton) complex, which physically connects the nuclear membrane and lamina to the cytoskeleton (Crisp *et al.*, 2006). Lamins A/C also interact with nucleoplasmic proteins such as barrier-to-autointegration factor (BAF), which prevents viral integration, and chromatin remodeling complexes, including the nucleosome remodeling and histone deacetylation component retinoblastoma-binding protein 4 (Montes de Oca *et al.*, 2009; Pegoraro *et al.*, 2009). In some cases, interaction with nucleoplasmic proteins serves to sequester proteins to the nuclear periphery, thus reducing the nucleoplasmic concentration. For example, lamin A physically interacts with the transcription factor Fos and retains it at the nuclear lamina, leading to suppression of activating protein-1–dependent transcription (Ivorra *et al.*, 2006; Gonzalez *et al.*, 2008).

Mutations in the *LMNA* gene cause a heterogeneous set of human diseases. More than 300 *LMNA* mutations have been identified and causally linked to >15 distinct diseases, which are referred to as laminopathies (Szeverenyi *et al.*, 2008; Dittmer and Misteli, 2011). The laminopathic disease mutations are distributed throughout the *LMNA* gene and show little correlation to disease type (Szeverenyi *et al.*, 2008; Dittmer and Misteli, 2011). A prominent hallmark of laminopathies is their high tissue specificity. Among the laminopathies, Emery–Dreifuss muscular dystrophy (EDMD), limb girdle muscular dystrophy 1B (LGMD1B), and dilated cardiomyopathy 1A (CMD1A) primarily affect muscle, whereas Dunnigan-type familiar partial lipodystrophy (FPLD) affects adipose tissue, and Charcot–Marie–Tooth neuropathy 2B1 (CMT2B1) impairs function of the peripheral nervous system (Rankin and Ellard, 2006; Worman and Bonne, 2007). A second class of laminopathies involves multiple tissues in different combinations, such as mandibuloacral dysplasia with type A lipodystrophy (MADA) and Hutchinson–Gilford progeria syndrome (HGPS; Rankin and Ellard, 2006; Worman and Bonne, 2007).

How mutations in *LMNA* cause disease and why many laminopathies are highly tissue specific are unclear and particularly intriguing, given that lamins A/C are expressed in most adult tissues (Rober *et al.*, 1989). One model for the tissue specificity of laminopathies proposes that variants of lamins A/C may affect interactions with proteins that are themselves expressed in a tissue-specific manner (Schirmer and Gerace, 2005). In support, nuclear envelope proteomes are highly variable among tissues (Korfali *et al.*, 2012). However, connecting altered lamin A/C protein interactions to clinically relevant molecular mechanisms remains a challenge.

To gain insights into the pathological mechanisms involved in laminopathies, we sought to systematically identify lamin A–interacting proteins whose binding is affected by disease-linked mutations. We screened an unbiased human ORFeome library comprising >12,000 genes to identify lamin A/C–binding proteins and probed their interaction with a comprehensive panel of 89 disease-linked lamin A variants. Our screening efforts identified novel lamin A/C-interacting proteins whose interaction is disrupted by laminopathy disease mutations, revealed lamin A/C residues important for protein–protein interactions, and identified disease-specific lamin A interactions at multidisease mutation sites. Our results support the notion that the tissue specificity of laminopathies is strongly driven by loss of tissue-specific lamin A/C interactions.

RESULTS

Systematic identification of lamin A–interacting proteins

To identify lamin A–interacting proteins in an unbiased manner, we performed a yeast two-hybrid (Y2H) screen using the human ORFeome V5.1 library, which contains 15,483 cloned open reading frames (ORFs), corresponding to 12,794 nonredundant human genes (a complete list of ORFs is available at http://horfdb.dfci.harvard.edu/hv5/). The library represents a comprehensive collection of ORFs and provides higher coverage than traditional Y2H libraries, the composition of which is limited by the gene expression pattern of the source tissue or cells from which the cDNA library is prepared, a potentially limiting factor when attempting to identify tissue-specific lamin A interactors (Bonaldo *et al.*, 1996; Maier *et al.*, 2011). The ORFeome library also ensures equal representation of each gene, in contrast to traditional Y2H libraries, in which the abundance of each clone in the library reflects its endogenous expression level. Because each ORFeome construct is sequence verified, the rate of false positives due to out-of-frame clones and mutations is minimized.

Each ORFeome clone was introduced into two Y2H expression vectors to generate a complete library of protein fusions between the ORF and Gal4 DNA–binding domain (DB-Y) and the Gal4 activation domain (AD-Y; Lamesch *et al.*, 2007). Conversely, 41 unique lamin A fragments (Supplemental Table S1A), all of varying size and encoding different combinations of lamin A domains, were introduced into Y2H expression vectors to generate protein fusions with the Gal4 activation domain (AD-lamin A) or the Gal4 DNA–binding domain (DB-lamin A). The use of multiple lamin A fragments increases the throughput of candidate protein identification and ameliorates potential cytotoxic effects. DB and AD constructs were transformed into the haploid *Saccharomyces cerevisiae* strains Y8930 (*MAT*α) and Y8800 (*MAT*a), respectively, and two complementary screening strategies were performed (Figure 1A; Dreze *et al.*, 2010). In a "forward" screen, 85 plates, each containing a different pool of 188 AD-ORFeome constructs, were tested against individual DB-lamin A constructs arrayed on a single plate (Figure 1A). In a "reverse" screen, the 41 AD-lamin A constructs were pooled and tested against individual DB-ORFeome constructs, which were arrayed across 147 plates (Figure 1A). Each screen was performed twice, and putative interactors were identified based on growth on selective media (see *Materials and Methods*; Dreze *et al.*, 2010). As a control, yeast were replica plated onto media containing cycloheximide, which counterselects for the AD vector and aids in identifying DB-Y autoactivating proteins (Dreze *et al.*, 2010). Approximately 1.2 million protein–protein combinations were tested, and

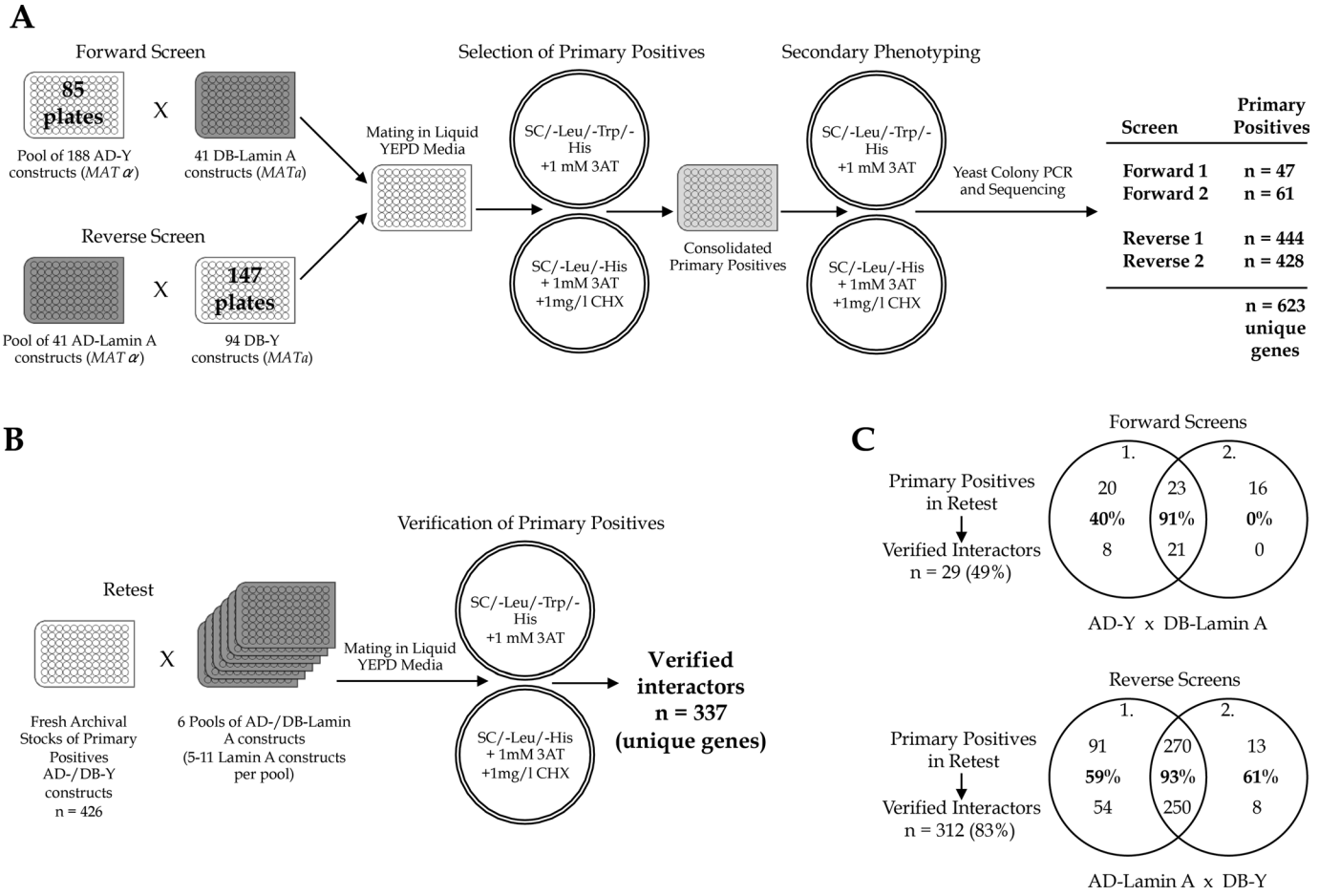

FIGURE 1: Yeast two-hybrid screen design and results. (A) Schematic of primary screen strategy. In the forward screen, 188 *MAT*α yeast, each transformed with a unique AD-Y construct (where Y is an ORFeome clone), are pooled, and an aliquot is deposited into 85 96-well plates. *MATa* yeast, each transformed with a unique DB-lamin A construct (41 in total), are also deposited in 96-well plates such that each well contains a unique DB-lamin A construct. Yeast are then mated in liquid YEPD medium (188 × 1). In the reverse screen, 41 *MAT*α yeast, each transformed with a unique AD-lamin A construct, are pooled and deposited into 96-well plates. *MATa* yeast, each transformed with a unique DB-Y construct, are deposited into 147 96-well plates so that each well contains a unique DB-Y construct. Yeast are then mated in liquid YEPD medium (41 × 1). After the mating reaction, yeast are plated in duplicate on SC/-Leu/-Trp/-His +1 mM 3-AT to select for interactors and SC/-Leu/-His, +1 mM 3-AT +1 mg/L cycloheximide (CHX) to select for autoactivators. Primary positive colonies are consolidated into 96-well plates containing liquid SC/-Leu/-Trp media, cultured overnight, and then replated on selection plates for secondary phenotyping. Colony PCR was performed for each primary positive, and the results were sequenced. Each screen was repeated twice and identified 623 unique interactors. (B) Schematic of the retest strategy. Fresh archival stocks of 426 unique primary positives are retested against pools of AD/DB-lamin A. Of these, 337 retested positive and are considered verified interactors. (C) Venn diagram of the retest results. Of the primary positives, 49% from the forward screen retested and 83% of the primary positives in the reverse screen retested. Primary positives identified in both screens (forward or reverse) retested at higher rates than those only identified in a single screen.

positive yeast colonies were cultured and replated on selective and control media for secondary phenotyping. Only colonies that continued to grow on selective media, and not on control media, were considered primary hits. The identity of the primary hits was verified by yeast colony PCR amplification of the insert and end-read sequencing.

Overall 623 unique interactors were identified in the four screens (Figure 1A and Supplemental Table S2). As expected, the forward screen was less sensitive (~50 hits/replica) compared with the reverse screen (~420 hits/replica) due to decreased sampling, with more constructs screened per well in the forward screen (188 AD-ORFeome constructs vs. 41 AD-lamin A constructs). In addition, reporter sensitivity is lower in the forward screen because DB-lamin A acts as a transcriptional repressor when tethered to the *GAL4* promoter (Lee *et al.*, 2009). Of the 623 primary positives identified, 426 were retested in the Y2H assay with fresh archival stocks of the ORFeome library, resulting in 337 (79%) validated interactors (Figure 1, B and C, and Supplemental Table S1, C and D; see *Materials and Methods*). Four interactors (CCDC120, CMTM5, LMNA, and TRIM39) were identified in all four screens, and six interactors (AGTRAP, ARL6IP1, PIK3R2, SCARA3, STX4, and TOR1AIP1) were identified in three of the four screens and all validated in retests. We identified 333 interactors in two of four screens, and of 281 of these interactors 258 (~92%) validated. Two hundred eighty interactors were identified in only one of four screens, and of 135 of these, 69 (~51%) validated in retesting. Thirteen of the identified

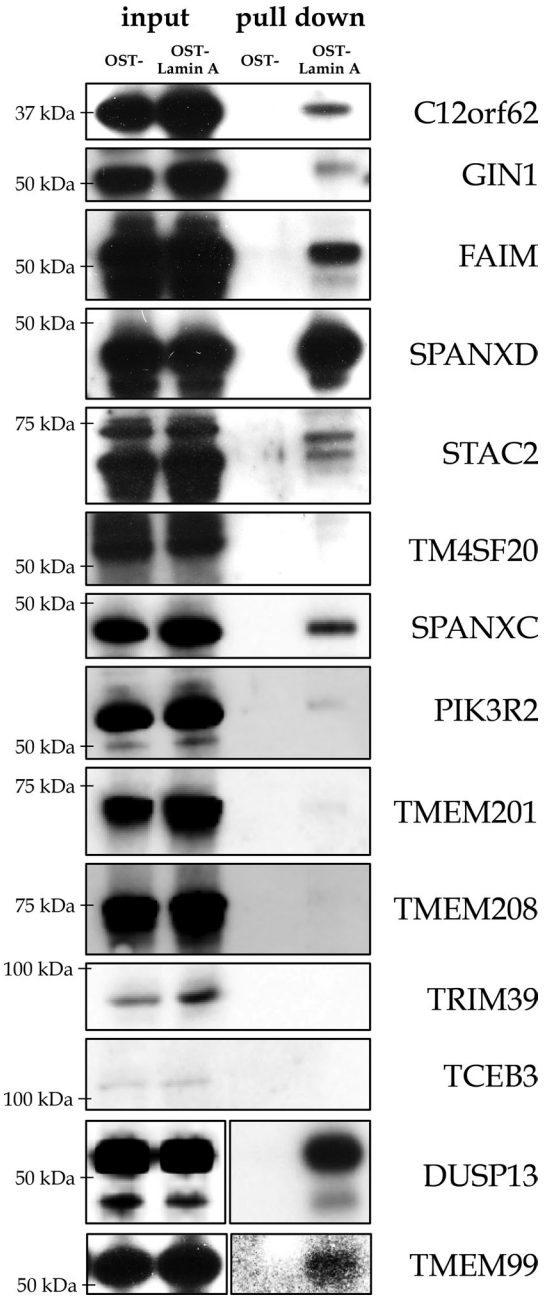

FIGURE 2: Validation of Y2H-verified interactors by pull-down assay. Validation of lamin A interactors in U2OS cells that stably express OneStrepTag-lamin A fusion (OST-Lamin A) or, as a negative control, OneStrepTag alone (OST). The U2OS cells were transfected with YFP fusions to the indicated proteins. Pulled-down proteins were detected using anti-GFP.

interactors, including LMNA, LMNB1, LMNB2, TMPO, and PCNA, had previously been reported as lamin A–interacting proteins, confirming the quality of the screening approach (Shumaker *et al.*, 2008).

A subset of interactors was chosen randomly for biochemical validation in pull-down assays using N-terminally yellow fluorescent protein (YFP)-tagged interactors expressed in U2OS cell lines that stably express OneStrepTag-lamin A fusion (OST-lamin A) or OneStrepTag alone (OST; Figure 2; Kubben *et al.*, 2010). Twelve of 18 Y2H interactors were detectable in pull-down assays, which included known lamin A interactors such as LMNA itself, TMPO, and LMNB1, in addition to several of the novel lamin A interactors (Figure 2). These results demonstrate that the interaction data set is enriched for lamin A–interacting proteins.

Cellular localization of interactors

Given that lamin A accumulates prominently at the nuclear periphery, we tested the localization of a subset of 104 interactors by high-throughout microscopy after expression in U2OS cells of N-terminally YFP-tagged versions of the interactors (Figure 3 and Supplemental Table S2). The localization pattern of each candidate was visually scored and categorized according to the extent of NE accumulation and cellular localization (Figure 3A). Several known lamin A interactors were included in the visual screen, such as LMNA, LMNB1, LMNB2, and TMPO, which served as positive controls for NE accumulation, and untagged YFP alone, which served as a negative control. We found that 53% of interactors showed NE accumulation (Figure 3B) and 47% of interactors did not accumulate at the NE but were homogeneously distributed throughout the nucleus and/or cytoplasm (Figure 3B). Note that peripheral localization is not a prerequisite for lamin interactors, as lamin A is also present in the nuclear interior, and several bona fide lamin interactors are diffusely distributed throughout the nucleus (Hozak *et al.*, 1995; Dorner *et al.*, 2007). Of the interactors that accumulated at the NE, 17% were exclusively nuclear, whereas the remaining candidates localized to the nucleus and cytoplasm. Of the interactors that did not accumulate at the NE, only 8% were exclusively localized in the cytoplasm. (Figure 3B).

Identification of progerin-specific interactors

To apply the ORFeome screening strategy to a specific laminopathy, we analyzed the Y2H interactome of progerin, the lamin A isoform responsible for the premature aging syndrome HGPS (Eriksson *et al.*, 2003). Progerin is a dominant lamin A isoform generated by the G608G mutation, which activates an intronic alternative pre-mRNA splice site (Eriksson *et al.*, 2003). Owing to the activation of the internal splice site, progerin has a 50–amino acid deletion in the C-terminal tail, which leads to its permanent farnesylation (Glynn and Glover, 2005). Five progerin constructs of varying length were tested in the primary screen, and the resulting validated candidates were classified according to their interaction with lamin A and/or progerin (Supplemental Table S1C; see *Materials and Methods*). We identified 225 progerin-specific interactions, 51 proteins that interacted with both lamin A and progerin (Supplemental Table S1D), and 61 interactors that were specific to lamin A. Of 80 progerin-specific interactors tested for their cellular localization, 89% displayed NE staining (Figure 3C), compared with only 53% of lamin A (Figure 3B). Of interest, only 8% of progerin-specific interactors, which accumulated at the NE, were also localized exclusively in the nucleus, in contrast to 17% of lamin A–specific or lamin A/progerin interactors (Figure 3, B and C).

Gene Ontology (GO) analysis confirmed the notion that progerin-specific interactors are a distinct group of proteins from lamin A interactors. Whereas lamin A interactors were enriched for components of the NE and lamina (Figure 4A; $p < 1 \times 10^{-3}$), progerin-specific interactors comprised mostly integral and intrinsic membrane proteins and components of the endoplasmic reticulum (ER; Figure 4B; $p < 1 \times 10^{-3}$). The progerin-specific interactors were enriched for proteins with soluble *N*-ethylmaleimide–sensitive factor attachment protein receptor activity and channel and transmembrane transporter activity (Figure 4B; $p < 1 \times 10^{-3}$). Progerin-specific interactors were also enriched for proteins that function in vesicle-mediated transport, membrane organization,

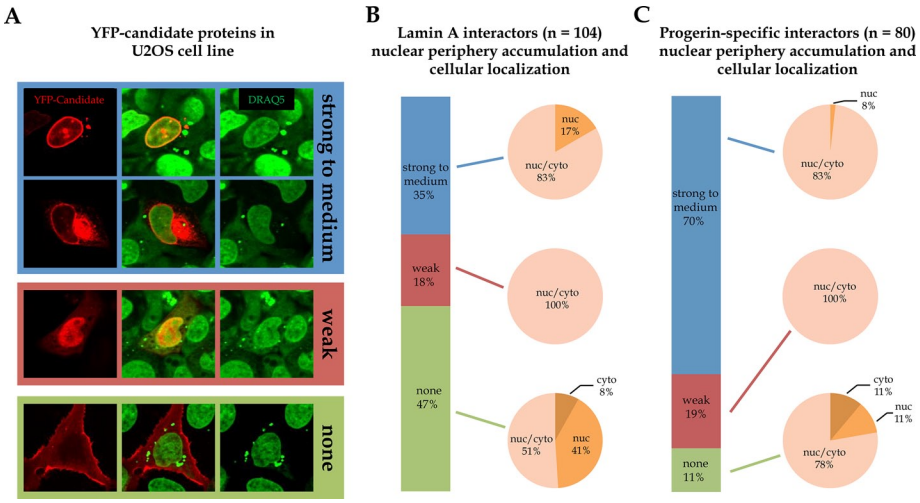

FIGURE 3: Localization of verified interactors. (A) Visual screen scoring for nuclear envelope accumulation. Each candidate was scored as strong to medium (blue), weak (red), or no (green) accumulation at the NE. (B) Localization pattern for lamin A interactors with respect to nuclear envelope accumulation and cellular localization (cyto, exclusively cytoplasmic; nuc, exclusively nuclear; nuc/cyto, both nuclear and cytoplasmic localization). (C) Localization pattern for progerin-specific interactors with respect to nuclear envelope accumulation and cellular localization.

transmembrane transport, and establishment of protein localization (Figure 4B; $p < 1 \times 10^{-3}$). The higher percentage of progerin-specific interactors that displayed NE staining compared with lamin A interactors might be explained by the preponderance of membrane-related components in this group, as high levels of membrane proteins might aggregate in the ER, which is continuous with the NE.

The observation that a higher percentage of progerin-specific interactors are not exclusively found in the nucleus but are also in the cytoplasm suggests that interactions may reflect pre–lamin A processing, which is thought to take place, in part, in the cytoplasm (Barrowman *et al.*, 2008). A key step in the maturation of lamin A is the addition and eventual removal of a C-terminal farnesyl group (Weber *et al.*, 1989), whereas progerin is permanently farnesylated (Glynn and Glover, 2005). To test for a potential role of farnesylation in the identified interactions, we probed progerin interactors against several lamin A variants impaired in farnesyl processing (Table 1). Of 223 progerin-specific candidates tested, none maintained its interaction with a progerin fragment containing a C661S mutation, which blocks transfer of the farnesyl moiety onto the terminal cysteine in lamin A or progerin (Table 1; Capell *et al.*, 2005). The effect of the C661S variant was specific to the progerin-only interactors and did not globally disrupt all interactions with progerin, since of the 27 candidates that interacted both with progerin and lamin A, 9 (33%) maintained their interaction with progerin C661S (Table 1). Conversely, of 220 progerin-specific interactors tested, 165 (75%) gained interaction with lamin A L647R, a variant that causes permanent farnesylation by blocking cleavage of the farnesyl group by the lamin A endoprotease ZMPSTE24 (Pendas *et al.*, 2002; Corrigan *et al.*, 2005; Glynn and Glover, 2005). These observations demonstrate that the majority of progerin interactions are mediated by its farnesylated C-terminus and that protein farnesylation is sufficient to mediate lamin A–protein interactions.

Systematic identification of interactors involved in laminopathies

Next we sought to identify disease-relevant interactors more broadly by testing a subset of 58 interactors, chosen based on their ability to interact robustly with multiple lamin A fragments, against a panel of 89 lamin A variants that represent 15 known laminopathies and are distributed throughout the lamin A protein (Figure 5 and Supplemental Table S3). We used the Y2H assay to test 4918 unique interactor–lamin A mutant binary pairs and identified 554 pairings that resulted in a loss of interaction (Figure 5 and Supplemental Table S3). The number of lost interactions among lamin A mutants ranged from 0 (0/42) to 75% (43/57; Figure 6; see later discussion).

Four of the lamin A mutants did not lose interaction with any of their binding partners. One of them, Arg377His, is located within the α-helical coiled coil 2B domain and is implicated in limb girdle

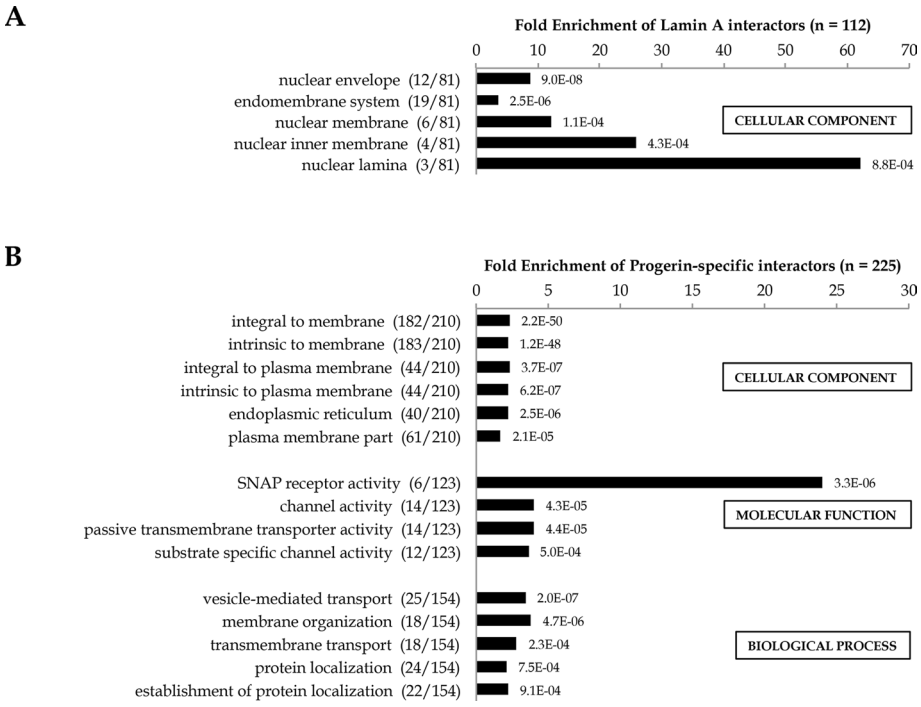

FIGURE 4: GO analysis. (A) Lamin A–interacting candidates and (B) progerin-specific candidates were analyzed for the GO categories cellular components (CC), biological process (BP), and molecular function (MF) against the ORFeome library as background. GO terms significantly enriched ($p < 1 \times 10^{-3}$) over background are listed next to the number of candidates annotated with the GO term over the total number of annotated candidates in each category.

AD-	DB-verified interactors: Progerin-specific interactors (n = 223)	DB-verified interactors: Lamin A and progerin interactors (n = 27)	AD-	DB-verified interactors: Progerin-specific interactors (n = 220)	DB-verified interactors: Lamin A and progerin interactors (n = 22)
Lamin A	0	27	Lamin A	0	22
Progerin	223	27	Progerin	220	22
Lamin A Cys661Ser	1	17	Lamin A Lys647Arg	165	22
Progerin Cys661Ser	0	9			

Two groups of DB-interactors were tested against AD-lamin A and AD-progerin constructs containing mutations affecting farnesylation. Numbers indicate how many DB-interactors interacted with each AD-lamin A or AD-progerin construct. Progerin-specific interactors only interact with farnesylated progerin. None of the 223 progerin-specific interactors interacted with AD-progerin Cys661Ser, a progerin variant that prevents farnesylation. Conversely, farnesylation of lamin A is sufficient to gain interaction with progerin-specific interactors. Of 220 progerin-specific interactors, 165 gained interaction with the lamin A Lys647Arg variant, which causes permanent farnesylation.

TABLE 1: Role of farnesylation in interactions.

muscular dystrophy D1, Emery–Dreifuss muscular dystrophy 2, and dilated cardiomyopathy 1A, whereas the remaining three, Asp136His, Glu145Lys, and Glu159Lys, are located within the α-helical coiled-coil 1B domain and are associated with HGPS (Muchir *et al.*, 2000; Eriksson *et al.*, 2003; Sebillon *et al.*, 2003; Reichart *et al.*, 2004; Garg *et al.*, 2009). Together with Ser143Phe, a fourth HGPS-associated lamin A variant, HGPS variants within the coiled-coil 1B domain had only a minimal effect, losing interaction with 2.5% of candidates compared with 17% for the rest of the variants in the coiled-coil 1B domain. The tendency of HGPS-associated variants to have little or no effect on protein–protein interactions supports a model in which disturbed assembly of lamin filaments, which leads to dominant gain-of-function effects, is the cause of HGPS (Goldman *et al.*, 2004; Dahl *et al.*, 2006). The effects of the HGPS-associated variants probably manifest as perturbations in higher-order filament formation, since none of the variants prevented lamin dimer formation (Supplemental Table S3).

Structure–function interaction analysis

The availability of a comprehensive library of lamin A mutants allowed mapping of the lamin A protein domains required for interactions. Of note, lamin A variants inside the immunoglobulin (Ig)-like fold domain lost interaction with more candidates than variants in the unstructured C-terminal tail (Table 2). The Ig-like fold domain is composed of two β-sheets that are closely associated in a β-sandwich (Dhe-Paganon *et al.*, 2002; Krimm *et al.*, 2002). The side chains of some residues orient toward the core of the domain and participate in stabilization of the β-sandwich through hydrophobic contacts and hydrogen bonds (Dhe-Paganon *et al.*, 2002; Krimm *et al.*, 2002). As expected, the most severely affected Ig-like domain mutants are two core variants, Leu454Pro and Asn456Lys, which lost interaction with 72 and 75% of candidates tested, respectively (Table 3). The third most severely affected Ig-like domain mutant was Arg455Pro, which lost interaction with 40% of candidates (Table 3). Unlike the side chains of Leu454 and Asn456, which are both positioned within the core of the Ig-like fold, a structural role of Arg455 has not been determined. The large effect of the Arg455Pro variant suggests that like Leu454 and Asn456, the side chain of Arg455 is oriented within the core and important for the stability of the Ig-like fold domain. Asn456Ile lost interaction with 18% of candidates, whereas Asn456Asp lost interaction with only 1% of candidates. The different effects for various Asn456 variants are likely a reflection of how the core domain accommodates the structural differences between amino acid side chains.

Side chains situated on the surface of the Ig-like fold domain, such as Trp482, are not predicted to affect the overall stability of the Ig-like fold domain, but are expected to affect protein–protein interactions (Dhe-Paganon *et al.*, 2002). Three different Trp482 variants, Trp482Gln, Trp482Leu, and Trp482Trp, lost interaction with 4% of candidates (Table 3), which is comparable to the 6% average of all solvent-exposed residues (Table 2). Overall lamin A variants whose substitutions affect core residues involved in maintaining the β-structure lost interactions with on average 20% of the candidates, compared with 6% for 8 variants affecting solvent-exposed residues and 9% for 15 variants affecting residues without a determined orientation, in line with a critical global role of the β-sheet structure in mediating interactions of lamin A with its partners (Table 2).

The relationship between the number of lost interactions and the location of lamin A mutations within the Ig-like domain fits a previously noted correlation of disease type and location of lamin A mutations within the Ig-like domain (Dhe-Paganon *et al.*, 2002). Our study included 23 variants that are predicted to affect the Ig-like domain core. Of these 21 are implicated in EDMD2, LGMD1B, CMD1A, and other types of muscular dystrophies and lose interaction with 20% of candidates. In comparison, of the eight variants in our study predicted to have surface-exposed residues, six cause FPLD2, HGPS, and MADA and lose interaction with only 6% of candidates. These results agree with the noted correlation between Ig-like fold structure and resulting diseases. Ig-like fold domain mutations associated with muscular dystrophies and cardiomyopathies generally affect core residues and disrupt overall protein stability, whereas mutations associated with lipodystrophies and progeria are surface-exposed residues and do not affect overall domain stability.

Interactors affected by laminopathy variants

In a converse approach, we asked how many interactions each lamin A interactor lost when tested against the panel of 83 lamin A mutants (Table 4). Of the 58 interactors tested, 50 lost interaction with at least one mutant (Table 4 and Figure 7). The interaction of eight candidates with lamin A was insensitive to lamin A mutations. Of importance, this group includes lamins LMNA, LMNB1, and LMNB2, suggesting that none of the variants significantly impairs lamin dimer formation mediated through the central coiled-coil domain. The other lamin A interactions that were insensitive to mutation were proliferating cell nuclear antigen (PCNA), reticulon 1/3 (RTN1/3), CREB3, and SENP2, suggesting that these proteins contain multiple, redundant lamin A interaction sites or that the relevant

FIGURE 5: Variant test summary heat map. Heat map summary of lamin A variant tests. The *y*-axis, laminopathy variants ($n = 89$); *x*-axis, interactors ($n = 58$). Green indicates no effect on interaction, red indicates a lost interaction, yellow indicates conflicting results between different lamin A fragments, and white indicates that no test was performed.

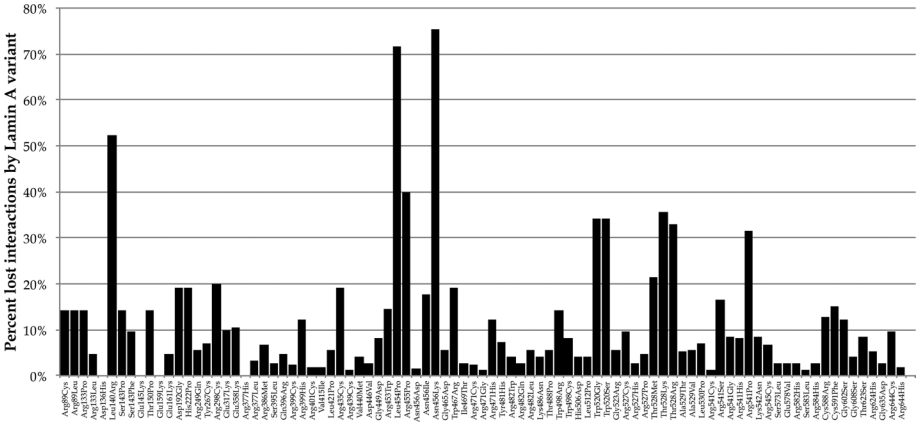

FIGURE 6: Percentage lost interactions, by lamin A variant. Bars represent the percentage of lost interactions for each variant. Variants are ordered numerically along the *x*-axis.

lamin A mutants that affect their interaction is not present in the panel. For the 50 interactors that lost binding with lamin A mutants, the number per candidate ranged from 1 to 72% (Table 4 and Figure 7). Of note are the combined losses of TMPO, TOR1AIP1, and DUSP13, which shared 10 mutant variants with which they lost interaction. Remarkably, 9 of the 10 variants cause CMD1A or EDMD2, which are diagnosed as separate diseases but have overlapping symptoms. Mutations in TMPO are known to cause CMDT1A, a cardiomyopathy, whereas DUSP13 and TOR1AIP1 have not previously been implicated in any diseases. All three interactors likely play a role, given the significant overlap among the candidates, the known association of TMPO with cardiomyopathies, and the similarities between EDMD2 and cardiomyopathies.

Disease-specific interactions at multidisease mutation sites

A remarkable feature of laminopathies is that phenotypically vastly distinct, tissue-specific diseases can be caused by differential amino acid substitutions of the same residue. A prominent example is Thr-528. Patients with Thr528Lys or Thr528Arg mutations suffer from muscular dystrophies, whereas Thr528Met causes progeria and a lipodystrophy as compound heterozygote with different lamin A variants (Bonne *et al.*, 2000; Raffaele Di Barletta *et al.*, 2000; Vytopil *et al.*, 2003; Savage *et al.*, 2004; Verstraeten *et al.*, 2006; Benedetti *et al.*, 2007; Yuan *et al.*, 2010; Scharner *et al.*, 2011; Saj *et al.*, 2012). To test whether emergence of distinct diseases is related to loss of interaction with distinct sets of proteins, we tested lamin A isoforms with the three Thr-528 substitutions against a panel of 57 interactors. We identified 35 interactors that lost binding with at least one of the Thr-528 variants (Supplemental Table S3). Remarkably, the candidates largely grouped by disease (Figure 8). Nineteen of the interactors lost association with the variants causing muscular dystrophies—Thr528Arg and Thr528Lys—but their interaction with Thr528Met, which causes HGPS and a lipodystrophy, was not affected. Conversely, 11 proteins lost interaction with the Thr528Met variant but not the Thr528Arg or Thr528Lys variants. The differential interaction properties correlate with the steric orientation of the mutant amino acids. The side chain of Thr-528 forms part of the core of the Ig-like fold domain, and substitutions, particularly with positively charged amino acids such as Arg and Lys, are predicted to disrupt folding and possibly reduce protein stability. In contrast, methionine, which is neutral and hydrophobic, more closely resembles threonine and is less likely to cause major structural changes.

Additional multidisease mutations exist in *LMNA*. Patients with Arg133Pro mutations develop EDMD2, and those with Arg133Leu mutations develop Werner syndrome (WS) or lipodystrophies. We identified two interactors, DUSP13 and TMPO, that specifically lost interaction with Arg133Pro but not Arg133Leu. Another multidisease mutation site is Arg541. Arg541His and Arg541Pro mutations cause EDMD2, whereas Arg541Cys, Arg541Ser and Arg541Gly primarily cause CMD1A. We identified one candidate, MTHFD2, that lost interaction with Arg541 variants associated with EDMD2 but

Lamin A/C protein domain	Variant tests	Lost interactions	Average lost interactions (%)
Coiled coil 1B	273	34	12
L12 linker	21	4	19
Coiled coil 2A	18	1	6
Coiled coil 2B	367	32	9
Tail (before nuclear localization signal)	268	11	4
Tail (nuclear localization signal)	73	4	5
Ig-like fold	2991	410	14
Core residues	1461	290	20
Solvent-exposed residues	534	31	6
Residue position not determined	996	89	9
Tail (after Ig-like fold)	907	58	6
	Total = 4918	**Total = 554**	**Average = 11**

Buried side chains predicted to be positioned within the core of the Ig-like fold domain: Val440Met, Leu454Pro, Asn456Asp, Asn456Ile, Asn456Lys, Trp467Arg, Ile469Thr, Arg471Cys, Arg471Gly, Arg471His, Tyr481His, Leu512Pro, Trp520Gly, Trp520Ser, Thr528Met, Thr528Lys, Thr528Arg, Leu530Pro, Arg541Cys, Arg541Ser, Arg541Gly, Arg541His, and Arg541Pro. Residues predicted to be solvent exposed in the Ig-like fold domain: Arg453Trp, Arg482Trp, Arg482Gln, Arg482Leu, Lys486Asn, Arg527Cys, Arg527His, and Arg527Pro.

TABLE 2: Summary of lost interactions, by lamin A/C protein domain.

Variant	Laminopathy	Lamin A 2–664			Lamin A 259–664			Lamin A 388–664			Total		
		Verified interactors	Lost interactions	%	Verified interactors	Lost interactions	%	Verified interactors	Lost interactions	%	Verified interactors	Lost interactions	%
Coiled coil 1B		**273**	**34**	**12**							**273**	**34**	**12**
Arg89Cys	EDMD2	21	3	14							21	3	14
Arg89Leu	CMD1A	21	3	14							21	3	14
Arg133Pro	EDMD2	21	3	14							21	3	14
Arg133Leu	WS, FPLD2, lipoatrophy syndrome	21	1	5							21	1	5
Asp136His	HGPS	21	0	0							21	0	0
Leu140Arg	WS	21	11	52							21	11	52
Ser143Pro	CMD1A	21	3	14							21	3	14
Ser143Phe	EDMD2, HGPS	21	2	10							21	2	10
Glu145Lys	HGPS	21	0	0							21	0	0
Thr150Pro	EDMD2	21	3	14							21	3	14
Glu159Lys	HGPS	21	0	0							21	0	0
Glu161Lys	CMD1A, DCM-CD	21	1	5							21	1	5
Asp192Gly	CMD1A, DCM-CD	21	4	19							21	4	19
L12 linker		**21**	**4**	**19**							**21**	**4**	**19**
His222Pro	EDMD2	21	4	19							21	4	19
Coiled coil 2A		**18**	**1**	**6**							**18**	**1**	**6**
Arg249Gln	EDMD2, LGMD1B	18	1	6							18	1	6
Coiled coil 2B		**126**	**21**	**17**	**241**	**11**	**5**				**367**	**32**	**9**
Tyr267Cys	EDMD2, CMD1A	21	2	10	7	0	0				28	2	7
Arg298Cys	CMT2B1	21	10	48	39	2	5				60	12	20
Glu317Lys	CMD1A	21	3	14	39	3	8				60	6	10
Glu358Lys	EDMD2, CMD, dropped head syndrome	18	2	11	39	4	10				57	6	11
Arg377His	LGMD1B, CMD1A, EDMD2,	3	0	0	39	0	0				42	0	0
Arg377Leu	LGMD1B, ADSMA, CMD1A, MD	21	2	10	39	0	0				60	2	3
Arg386Met	EDMD2	21	2	10	39	2	5				60	4	7
Tail (before NLS)		**84**	**8**	**10**	**106**	**3**	**3**	**78**	**0**	**0**	**268**	**11**	**4**
Ser395Leu	Metabolic syndrome	18	1	6	7	0	0	13	0	0	38	1	3
Gln396Arg	EDMD2	21	2	10	7	0	0	13	0	0	41	2	5
Arg399Cys	FPLD2, CMD1A	21	1	5	7	0	0	13	0	0	41	1	2
Arg399His	Metabolic syndrome	21	3	14	7	2	29	13	0	0	41	5	12
Arg401Cys	EDMD2				39	1	3	13	0	0	52	1	2
Val415Ile	LAF	3	1	33	39	0	0	13	0	0	55	1	2
NLS		**21**	**2**	**10**	**39**	**2**	**5**	**13**	**0**	**0**	**73**	**4**	**5**

TABLE 3: Summary of variant panel test, by lamin A variant.

Continues

Variant	Laminopathy	Lamin A 2–664			Lamin A 259–664			Lamin A 388–664			Total		
		Verified interactors	Lost interactions	%	Verified interactors	Lost interactions	%	Verified interactors	Lost interactions	%	Verified interactors	Lost interactions	%
Leu421Pro	Metabolic syndrome	21	2	10	39	2	5	13	0	0	73	4	5
Ig-like domain		**927**	**156**	**17**	**1531**	**248**	**16**	**533**	**6**	**1**	**2991**	**410**	**14**
Arg435Cys	HGPS, RD	21	13	62	39	1	3	13	0	0	73	14	19
Arg439Cys	FPLD2, metabolic syndrome	21	1	5	39	0	0	13	0	0	73	1	1
Val440Met	CMD1A	21	2	10	39	1	3	13	0	0	73	3	4
Asp446Val	EDMD2	21	1	5	39	1	3	13	0	0	73	2	3
Gly449Asp	EDMD2	21	0	0	39	6	15	13	0	0	73	6	8
Arg453Trp	EDMD2, LGMD1B	3	1	33	39	7	18	13	0	0	55	8	15
Leu454Pro	EDMD2	21	13	62	39	30	77				60	43	72
Arg455Pro	Dropped head syndrome	21	7	33	39	17	44				60	24	40
Asn456Asp	Dropped head syndrome	18	1	6	39	0	0	13	0	0	70	1	1
Asn456Ile	EDMD2	21	6	29				13	0	0	34	6	18
Asn456Lys	EDMD2	18	14	78	39	29	74				57	43	75
Gly465Asp	FPLD2	21	3	14	39	0	0	13	1	8	73	4	5
Trp467Arg	EDMD2	21	7	33	39	7	18	13	0	0	73	14	19
Ile469Thr	EDMD2	21	2	10	39	0	0	13	0	0	73	2	3
Arg471Cys	HGPS, MADA, RSS	21	1	5	7	0	0	13	0	0	41	1	2
Arg471Gly	FPLD2, FPLD1	21	1	5	39	0	0	13	0	0	73	1	1
Arg471His	CMD1A	21	2	10	7	3	43	13	0	0	41	5	12
Tyr481His	LGMD1B	21	3	14	7	0	0	13	0	0	41	3	7
Arg482Trp	FPLD2	21	2	10	39	1	3	13	0	0	73	3	4
Arg482Gln	FPLD2	21	2	10	39	0	0	13	0	0	73	2	3
Arg482Leu	FPLD2	21	3	14	39	1	3	13	0	0	73	4	5
Lys486Asn	FPLD2	21	3	14	39	0	0	13	0	0	73	3	4
Thr488Pro	LAF	21	2	10	39	2	5	13	0	0	73	4	5
Trp498Arg	EDMD2, CMD1A	21	2	10	7	2	29				28	4	14
Trp498Cys	LGMD1B	21	2	10	39	4	10	13	0	0	73	6	8
His506Asp	Metabolic syndrome	18	3	17	39	0	0	13	0	0	70	3	4
Leu512Pro	LGMD1B	21	2	10	39	1	3	13	0	0	73	3	4
Trp520Gly	EDMD2	21	2	10	39	22	56	13	1	8	73	25	34
Trp520Ser	EDMD2	21	3	14	39	21	54	13	1	8	73	25	34
Gly523Arg	CMD1A	21	2	10	39	2	5	13	0	0	73	4	5
Arg527Cys	HGPS, MADA	21	2	10	39	5	13	13	0	0	73	7	10
Arg527His	MADA	21	2	10	39	0	0	13	0	0	73	2	3
Arg527Pro	EDMD2, CMD1A, EDMD3	21	2	10	7	0	0	13	0	0	41	2	5

TABLE 3: Summary of variant panel test, by lamin A variant.

Continues

Variant	Laminopathy	Lamin A 2–664			Lamin A 259–664			Lamin A 388–664			Total		
		Verified interactors	Lost interactions	%	Verified interactors	Lost interactions	%	Verified interactors	Lost interactions	%	Verified interactors	Lost interactions	%
Thr528Met	HGPS, FPLD1	18	13	72	39	2	5	13	0	0	70	15	21
Thr528Lys	EDMD2, LGMD1B	21	3	14	39	23	59	13	0	0	73	26	36
Thr528Arg	EDMD2	21	3	14	39	21	54	13	0	0	73	24	33
Ala529Thr	MADA	18	2	11	7	0	0	13	0	0	38	2	5
Ala529Val	MADA	21	4	19	39	0	0	13	0	0	73	4	5
Leu530Pro	EDMD2	21	2	10	7	0	0				28	2	7
Arg541Cys	CMD1A, cardiac arrhythmia	21	0	0	39	1	3	13	0	0	73	1	1
Arg541Ser	CMD1A, EDMD2	21	9	43	39	2	5	13	1	8	73	12	16
Arg541Gly	CMD1A	18	0	0	39	5	13	13	1	8	70	6	9
Arg541His	EDMD2	21	2	10	39	3	8	13	1	8	73	6	8
Arg541Pro	EDMD2, MD	21	2	10	39	21	54	13	0	0	73	23	32
Lys542Asn	HGPS	18	2	11	39	4	10	13	0	0	70	6	9
Arg545Cys	EDMD2	21	2	10	39	3	8	13	0	0	73	5	7
Tail		**243**	**30**	**12**	**482**	**24**	**5**	**182**	**4**	**2**	**907**	**58**	**6**
Ser573Leu	CMD1A, LGMD1B, FPLD2	21	2	10	39	0	0	13	0	0	73	2	3
Glu578Val	HGPS	18	1	6	7	0	0	13	0	0	38	1	3
Arg582His	FPLD2	18	2	11	39	0	0	13	0	0	70	2	3
Ser583Leu	FPLD1	21	1	5	39	0	0	13	0	0	73	1	1
Arg584His	FPLD2	21	1	5	39	1	3	13	0	0	73	2	3
Cys588Arg	HGPS	18	1	6	39	7	18	13	1	8	70	9	13
Cys591Phe	FPLD2	21	5	24	39	6	15	13	0	0	73	11	15
Gly602Ser	Type A insulin resistance syndrome	21	9	43	39	0	0	13	0	0	73	9	12
Gly608Ser	HGPS	21	3	14	39	0	0	13	0	0	73	3	4
Thr623Ser	HGPS	18	2	11	39	4	10	13	0	0	70	6	9
Arg624His	EDMD2	3	0	0	39	2	5	13	1	8	55	3	5
Gly635Asp	CMD1A	18	1	6	7	0	0	13	0	0	38	1	3
Arg644Cys	CMD1A, HGPS, EDMD2, FPLD2, neuropathy	21	2	10	39	3	8	13	2	15	73	7	10
Arg644His	CMD1A	3	0	0	39	1	3	13	0	0	55	1	2
Grand total		**1713**	**256**	**15**	**2399**	**288**	**12**	**806**	**10**	**1**	**4918**	**554**	**11**

Results of lamin A variant panel tests according to variant. Variants are listed in ascending order, grouped by domain, and followed by the associated laminopathy. Variant panels were constructed in three different lamin A fragments: lamin A 2–664, lamin A 259–664, and lamin A 388–664. The number of validated interactors tested against each fragment for each variant is indicated, as well as the number that lost interaction. For a complete list see Supplemental Table S3. NLS, nuclear localization signal.

TABLE 3: Summary of variant panel test, by lamin A variant. Continued

maintained interaction with variants associated with CMD1A. We conclude that variants at multidisease sites that cause related diseases show specificity for interaction partners, possibly explaining the tissue specificity of their appearance.

DISCUSSION

Mutations in lamins and other proteins of the nuclear lamina have been linked to diverse pathologies ranging from muscular dystrophies to lipodystrophies, neuropathies, and progeroid aging

Fragment	Candidate	Variants introduced in fragment	Lost interactions	Interactions lost (%)
LMNA 2–664				
AD	DB-			
	CCNG1	83	21	25
	DUSP13	83	19	23
	FAIM	83	7	8
	LMNA	83	0	0
	LMNB1	83	0	0
	LMNB2	83	0	0
	MORF4L1	83	41	49
	MTHFD2	83	12	14
	PNKP	83	4	5
	TCEANC	83	7	8
	TCEB3	83	8	10
	TMEM199	83	1	1
	TMPO	83	11	13
	TOR1AIP1	83	18	22
	ZNF3	83	60	72
	ZNF439	83	14	17
	ZNF440	83	14	17
	ZNF69	83	6	7
	***n* = 18**		**Total = 243, average = 13.5**	**Average = 16**
DB	AD-			
	CCDC120	73	12	16
	LMNA	73	0	0
	PIAS2	73	1	1
	***n* = 3**		**Total = 13, average = 4.3**	**Average = 6**
LMNA 259–664				
AD	DB-			
	ABCA9	59	8	14
	ANXA6	59	8	14
	C12orf48	59	18	31
	C4orf6	59	13	22
	CENPP	59	20	34
	CETN3	59	8	14
	DDX43	59	11	19
	FAM164C	59	3	5
	FCER1A	59	7	12
	GIN1	59	16	27
	MTHFD2	59	7	12
	MYADM	59	9	15
	PKD2	59	10	17
	RANBP9	59	8	14
	RGS18	59	8	14
	SEC22A	59	7	12

TABLE 4: Summary of variant panel tests, by candidate.

Continues

Fragment	Candidate	Variants introduced in fragment	Lost interactions	Interactions lost (%)
	SENP2	59	0	0
	SIAH1	118[a]	23	19
	SLC30A8	59	5	8
	SPANXC	59	9	15
	SPANXD	59	7	12
	STAC2	59	8	14
	TCEANC	59	9	15
	TCEB3	59	4	7
	TM4SF20	59	11	19
	TMEM199	59	0	0
	TMEM74	59	4	7
	UBE2Q1	59	7	12
	ZNF138	59	9	15
	ZNF439	59	5	8
	ZNF569	59	8	14
	***n* = 31**		**Total = 270, average = 8.7**	**Average = 14**
DB	AD-			
	ARL6IP1	73	4	5
	CCDC120	73	4	5
	CCDC155	73	2	3
	IFFO1	73	2	3
	KPNA6	73	3	4
	PCNA	73	0	0
	RTN4	73	3	4
	***n* = 7**		**Total = 18, average = 2.6**	**Average = 4**
LMNA 388–664				
DB	AD-			
	AGTRAP	62	2	3
	ARL6IP1	62	0	0
	C20orf141	62	2	3
	CCDC155	62	0	0
	CREB3	248[a]	0	0
	DERL1	62	6	10
	PCNA	62	0	0
	RTN1	62	0	0
	RTN3	62	0	0
	RTN4	62	0	0
	***n* = 10**		**Total = 10, average = 1**	**Average = 2**
		Total = 4918	**Total = 554**	

Results of lamin A variant panel tests according to candidate. The Fragment column indicates which AD/DB-lamin A fragment fusion protein interacts with the corresponding AD/DB-candidate fusion. In the third column, the number of disease-associated variants introduced in each lamin A fragment is indicated, followed by the number of variants that caused a loss of interaction. The overall percentage of lost interactions per candidate is indicated in the last column.

[a]Combined results from multiple candidate isoforms.

TABLE 4: Summary of variant panel tests, by candidate. Continued

syndromes (Rankin and Ellard, 2006; Worman and Bonne, 2007). Although lamins A/C are widely expressed in most adult tissues, many of these diseases exhibit pronounced tissue specificity. It has been proposed that disrupted lamin A interactions with unidentified tissue-specific factors may mediate the development and tissue preferences observed in these diseases (Schirmer and

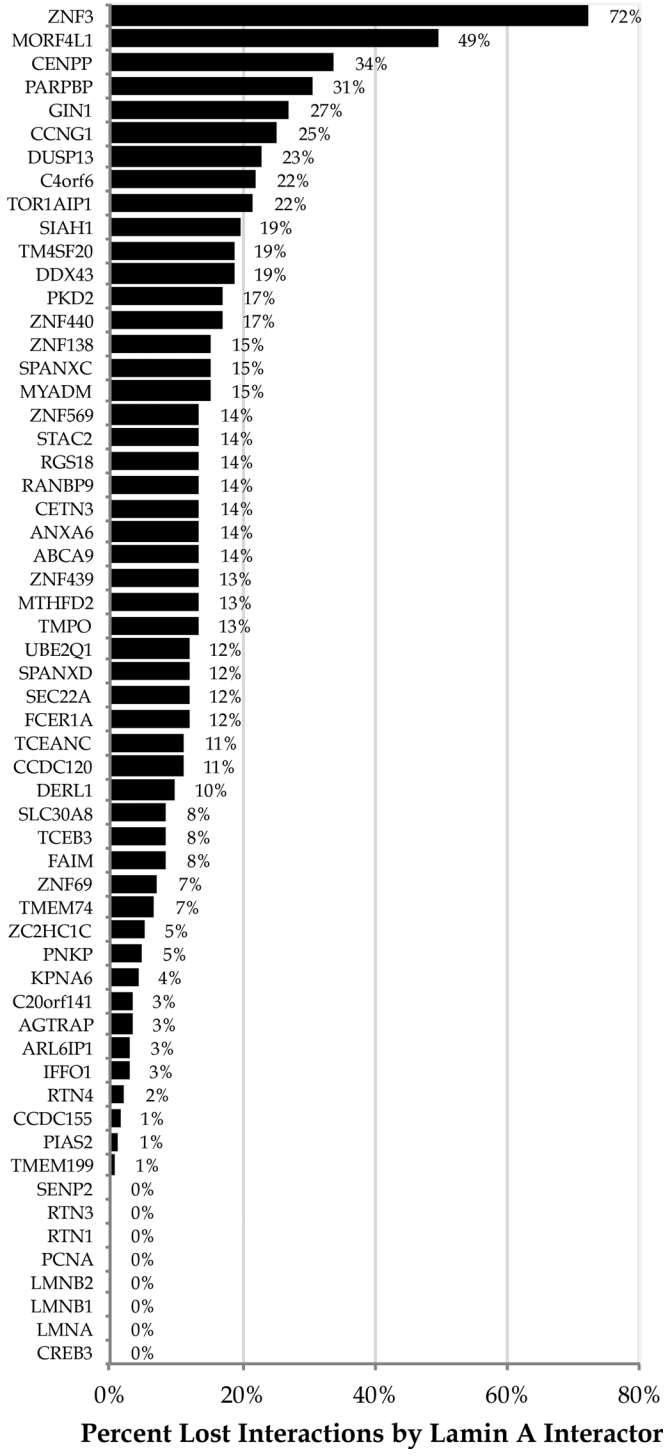

FIGURE 7: Percentage lost interactions, by lamin A interactor. Bars represent number of lost interactions as a percentage of all interactors tested for individual variants. Candidates are ranked according to their percentage of lost interactions.

Gerace, 2005). This model is in line with the observed high degree of tissue specificity of the NE proteome (Korfali *et al.*, 2012). To unravel the pathogenic mechanisms in laminopathies, we screened an unbiased ORFeome library to identify lamin A interactors and systematically evaluated their interaction with 89 different lamin A disease variants.

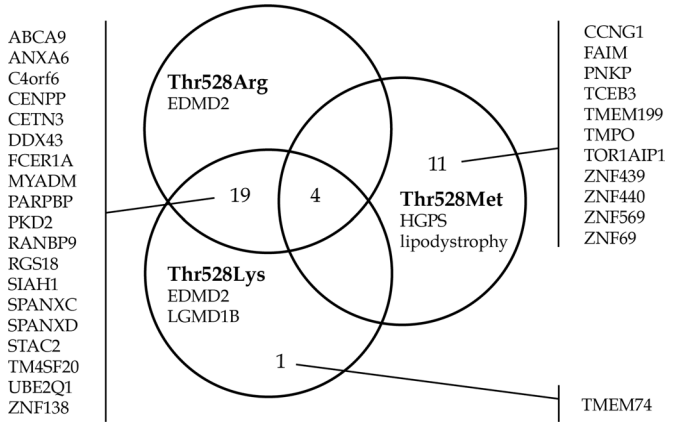

FIGURE 8: Disease-specific interactions at Thr-528 variants. Venn diagram of 35 candidates that lost interaction with Thr-528 variants. Nineteen of the candidates lost interaction only with Thr528Arg and Thr528Lys, which cause muscular dystrophies. Eleven of the candidates lost interaction with only Thr528Met, which causes HGPS and lipodystrophy.

We identified and validated 337 proteins that interact with lamin A or progerin. Reassuringly, the lamin A interactors included many known interactors, were significantly enriched for components of the lamina, NE, and NE membrane, and preferentially localized to the nuclear periphery. The high validation rate in orthogonal pull-down assays suggests that our set of candidates contains a significant number of genuine lamin A interactors. Comparison of the Y2H candidates with available NE proteomic data sets obtained from muscle and liver tissues and blood leukocytes indicated that of the 337 candidates, 35% are also found in NE biochemical fractions (Korfali *et al.*, 2012). It is important to note that the characterization of the NE proteome is incomplete and is variable across different tissue and cell types. Only 16% of NE proteins overlap between muscle, liver, and leukocytes, suggesting that the actual overlap between our candidates and the NE proteome is higher (Korfali *et al.*, 2012).

We identified 102 lamin A interactors, several of which are associated with at least one of the laminopathies or related diseases. These include LMNB2, which is associated with an acquired lipodystrophy, and TMPO, 2-actin, phospholamban, transmembrane protein 43 (TMEM43/LUMA), and vesicle-associated membrane protein 1/synaptobrevin 1, which are implicated in cardiomyopathies and other heart diseases. Whereas LMNB2 maintained its interaction with all lamin A variants, TMPO lost interaction with 11 variants, 9 of which cause cardiomyopathies or muscular dystrophies. It will be important to investigate the involvement of TMPO in cardiomyopathies caused by mutations in *LMNA*, particularly those identified here.

In addition, our approach has the potential to identify novel disease-relevant candidate proteins in an unbiased manner. One lamin A interactor, annexin VI (ANXA6), lost interaction with eight variants located within the Ig-like domain. Seven of the variants are buried within the core and cause EDMD2, whereas the orientation of the remaining variant is unknown and causes CMD1A. These findings dovetail with indications that ANXA6 may have a role in cardiomyopathies. Annexins are Ca^{2+} effectors that mediate cellular responses to changing intracellular levels of calcium, and elevated intracellular calcium concentrations cause the translocation of several annexins, including ANXA6, to the plasma membrane and nuclear envelope (Skrahina *et al.*, 2008). Proteomic studies show that ANXA6 is a

component of the NE in muscle, liver tissue, and blood cells (Korfali *et al.*, 2012). Overexpression of ANXA6 in cardiomyocytes of a transgenic mouse model causes hypertrophy and heart failure (Gunteski-Hamblin *et al.*, 1996). During end-stage heart failure, levels of ANXA6 decrease in cardiomyocytes, whereas other annexins show increased levels (Jans *et al.*, 1998). This has led to the view that down-regulation of ANXA6 during heart failure creates a framework that favors improved cardiomyoctye function (Gunteski-Hamblin *et al.*, 1996). The involvement of ANXA6 in cardiomyopathies and muscular dystrophies warrants further study.

We tested 89 lamin A variants against 58 of the candidates that interact with lamin A, and we generated a comprehensive map of effects of variants on protein–protein interactions. This data set allowed us to understand which residues and protein domains are important for protein–protein interactions. Approximately half of the N-terminal portion of lamin A protein consists of coiled-coil domains. Mutations within the coiled-coil domains, including the linkers, lost interaction with on average 10% of candidates. The coiled-coil domain mediates dimerization with other lamins, but none of the lamins lost interaction with any of the variants, indicating that none of the variants participates in dimerization. The C-terminal half of lamin A, excluding the Ig-like domain, is unstructured and lost interaction with on average ~6% of candidates. Except for a nuclear localization signal, the function of the unstructured domain is not well understood. Structural studies of the Ig-like domain indicate that residues whose side chains are oriented toward the core are crucial for stabilization of the β-sandwich (Dhe-Paganon *et al.*, 2002; Krimm *et al.*, 2002). Consistent with the structural predictions, core variants lost interactions with on average 20% of candidates, compared with 6% of candidates for variants on the domain surface.

Systematic screening of known disease mutations has the potential to provide novel insights into disease mechanisms. The identification of a disproportionate number of progerin-specific interactors was unexpected, since only 5 of 41 lamin A constructs used in the primary screen contain the disease-relevant 50–amino acid deletion. The identification of gain-of-function progerin interactors is consistent with models of HGPS, which envision a dominant effect of progerin (Goldman *et al.*, 2004; Dahl *et al.*, 2006). Of interest, the 225 progerin-specific interactors were significantly enriched for membrane proteins, possibly reflecting a contribution of the C-terminal farnesyl group to their interactions. Conversely, 61 of 112 (54%) lamin A interactors lost interaction with progerin. Of the eight candidates that did not lose interaction with any of the missense lamin A variants, five lost interaction with progerin, including CREB3, PCNA, LMNB2, and two reticulons, RTN1 and RTN3. RTN4, a third reticulon, and ARL6IP1, a candidate that also contains the reticulon homology domain (RHD), also lost interaction with progerin. In variant tests with lamin A missense mutations, RTN4 and ARL6IP1 lost interactions with only 2 and 3% of candidates, respectively (Figure 7), suggesting that the proteins containing the RHD are largely insensitive to laminopathy missense mutations but are sensitive to the deletion in progerin. Reticulons and ARL6IP1 have membrane-shaping activity, function as ER-shaping proteins (Yang and Strittmatter, 2007; Yamamoto *et al.*, 2014), and also function in NE assembly by regulating the contribution of ER tubules to the nascent NE and in subsequent NE expansion (Anderson and Hetzer, 2008). Nuclei from HGPS patients are lobulated and misshapen, which may indicate dysfunctional NE reformation and expansion.

Why different substitutions of the same lamin A residue cause vastly different diseases is an enigmatic feature of the laminopathies. In our Y2H analyses, multimutation residues that cause distinct diseases, such as Arg-133, Thr-528, and Arg-541, led to disease-specific loss of distinct sets of interactors. The results substantiate the genetics of laminopathy patients with molecular evidence, demonstrating that different substitutions of the same residue can have profoundly different effects on lamin A protein function. Identification of disease-specific candidates is a foothold for future functional studies and clinical efforts.

Lamin A/C is at the crossroads of many nuclear processes, and mutations cause a large number of diverse diseases. It is becoming increasing clear that the molecular functions of lamin A/C go far beyond its traditional role as a structural element and involve an extensive number of lamin A/C binding partners. Systematic identification of these interaction partners will provide the basis for the functional analysis of lamin A and its disease-causing mutants.

MATERIALS AND METHODS

Cloning, yeast transformations, and pool preparations

Fragments of lamin A were amplified from cDNA using PfuUltra II Fusion HS DNA Polymerase (Agilent Technologies, Santa Clara, CA), cloned into the pDONR223 (Life Technologies, Carlsbad, CA) vector, and then verified by sequencing. See Supplemental Table S1A for a list of all lamin A fragments. pDONR223-lamin A fragments were then cloned into pAD/pDB vectors using LR Clonase II Plus enzyme (Life Technologies). Yeast strains Y8800 and Y8930 were transformed with pDB-lamin A and pAD-lamin A vectors, respectively, using a lithium acetate transformation protocol (Dreze *et al.*, 2010). An AD pool of 41 different pAD-lamin A fragment constructs transformed in Y8800 was constructed as described in Dreze *et al.* (2010).

Yeast two-hybrid screen

Screening was performed essentially as described in Dreze *et al.* (2010). Before the screen, the AD-/DB-lamin A constructs were tested to ensure that none of the fusion proteins were autoactivators. Glycerol yeast stocks of the DB-X (Y8930) or AD-pool (Y8800) strains were used to inoculate 96-well plates containing liquid selective media (SC/-Leu or SC/-Trp). Plates were incubated at 30°C for 3 d with agitation. For the mating reaction, 5 µl of opposite-mating-type strains was combined in 96-well plates containing 160 µl of liquid yeast extract/peptone/dextrose (YEPD) per well and incubated overnight at 30°C with shaking. A 5-µl amount of each mating reaction was replica plated onto SC/-Trp/-Leu/-His + 1 mM 3-amino-1,2,4-triazole (3-AT) media (screening plate) and SC/-Leu/-His + 1 mM 3-AT + 1 mg/l cycloheximide media (de novo autoactivator plate). Each set of plates was incubated at 30°C for 3 d and scored for primary positives. Primary positives were defined as having a growth phenotype on the screening plate and a negative growth phenotype on the corresponding de novo autoactivator plate. Primary positive colonies were picked from the screening plate with sterile toothpicks and used to inoculate 96-well plates containing 160 µl of liquid SC/-Leu/-Trp media per well and then grown for 2 d at 30°C. Then 5 µl of culture from the SC/-Leu/-Trp plate was spotted onto fresh selective agar medium plates and de novo activator plates to verify the primary positive phenotype (phenotyping II). After 3 d, plates were again scored for secondary positives, which were then used to inoculate 96-well plates containing 160 µl of fresh liquid SC/-Leu/-Trp media per well and grown for 2 d at 30°C. Sequence identification of primary positives was performed by yeast colony PCR, followed by sequencing of the PCR product. To reduce false-positive rate and improve the quality of the interaction data set,

primary positives were retested in the Y2H assay using fresh archival stocks of the ORFeome library. This archival library was prepared independently from the library used in the primary screen and helps to reduce the number of false positives caused by *cis*- or *trans*-acting mutations. Of the 623 primary positives in the primary screen, 426 (68%) were present in the retest. These primary positives were then tested against lamin A using a pooling strategy similar to that used in the primary screen, except that the 41 lamin A constructs were divided into six subpools in which each pool was assigned 5–11 lamin A constructs (note that 7 additional lamin A constructs not in the primary screen were included in the retest; see Supplemental Table S1, C and D, for composition of each pool and retest results). The six AD/DB-lamin A subpools were individually tested against the 426 AD/DB-ORFeome primary positive candidates (Figure 1B). If the candidate scored positive with at least one of the six lamin A subpools, it was considered verified.

Transfections and pull-down assay

U2OS cells stably expressing OneSTrEP-tagged lamin A (OST-lamin A) or the OneSTrEP epitope alone (OST; IBA, Goettingen, Germany) were grown until ~90% confluence in 150-mm plates. Cells were transfected with YFP-candidate fusion constructs (pEYFP candidate) using GenJet reagent according to the manufacturer's instructions. After 24 h, cells were subjected to the pull-down procedure as previously described (Kubben *et al.*, 2010). We added 2× NuPAGE loading buffer (Life Technologies) to washed STrEPtactin matrix (IBA, Goettingen, Germany) and then heated it at 95°C for 20 min to elute precipitated proteins.

GO analysis

GO analysis of interactors was performed for GO categories cellular components, biological process, and molecular function using ORFeome v5.1 (http://horfdb.dfci.harvard.edu/hv5/) as background (Huang da *et al.*, 2009). Entrez Gene IDs were used as input, and the default Database for Annotation, Visualization, and Integrated Discovery settings were used for analysis.

Western blot

Samples were resolved on NuPAGE Bis-Tris Precast 4–12% gels (Life Technologies) and then blotted on polyvinylidene fluoride membranes (EMD Millipore, Billerica, MA). Membranes were blocked for 1 h in blocking buffer (5% bovine serum albumin, 20 mM Tris-HCl, pH 7.5, 150 mM NaCl, 0.1% Tween-20) and then incubated overnight at 4°C with anti-GFP antibody (Life Technologies) diluted 1:2000 with blocking buffer. The membranes were washed three times for 15 min with TBS-T (20 mM Tris-HCl, pH 7.5, 150 mM NaCl, 0.1% Tween-20) and incubated with horseradish peroxidase–labeled anti-mouse (ECL mouse IgG; GE Healthcare, Little Chalfont, United Kingdom) diluted 1:5000 with blocking buffer for 1 h at room temperature and washed as before. Proteins were detected with Amersham ECL Plus Western Blotting reagent (GE Healthcare). Aliquots of pre–pull-down cell lysate for each sample were analyzed for levels of β-tubulin to ensure uniform protein levels.

Localization of candidates

The pEYFP-Y candidate constructs used in the visual screen were made by using available pAD/pDB-Y clones from the yeast ORFeome library. Yeast minipreps were performed using Zymoprep Yeast Plasmid Miniprep II (Zymo Research, Irvine, CA) according to the manufacturer's instructions. Rescued plasmids were transformed into TOP10-competent cells (Life Technologies), and candidate ORFs were amplified using miniprep DNA as template with PfuUltra II Fusion HS DNA Polymerase, using the forward primers AD (5′-CGCGTTTGGAATCACTACAGGG-3′) and DB (5′-GGCTTCAGTGGAGACTGATATGCCTC-3′), and the reverse primer Term (5′-GGAGACTTGACCAAACCTCTGGCG-3′). PCR products were recombined into a Gateway compatible pEYFP vector using LR Clonase II Plus enzyme (Life Technologies). Sequence-verified pEYFP constructs were transfected using GenJet In Vitro DNA Transfection Reagent (SignaGen Laboratories, Rockville, MD) into U2OS cells in 96-well clear-bottom microplates according to the manufacturer's instructions. Cells were fixed 48 h posttransfection with 4% paraformaldehyde in phosphate-buffered saline and stained with DRAQ5 (Cell Signaling Technology, Danvers, MA). Confocal fluorescence images of multiple fields from each well were captured using the CellVoyager CV6000 high-content microscopy system (Yokogawa Electric Corporation, Tokyo, Japan) and analyzed using ImageJ software (National Institutes of Health, Bethesda, MD).

Y2H lamin A–variant panel construction

A series of laminopathy variants was created in three fragments of lamin A: lamin A 2–664, lamin A 259–664, and lamin A 388–664. Mutations were introduced into fusion PCR products by site-directed mutagenesis (for a complete list of primers and variants see Supplemental Table S4), which were subsequently recombined into pDONR223 using BP Clonase and then verified by sequencing (Suzuki *et al.*, 2005; Charloteaux *et al.*, 2011). This resulted in three variant panels: 1) pDONR223-lamin A 2–664 (n = 88 variants), 2) pDONR223-lamin A 259–664 (n = 73 variants), and 3) pDONR223-lamin A 388–664 (n = 62 variants). Collectively the three panels comprise 223 unique pDONR223-lamin A constructs and represent 89 unique laminopathy variants. The pDONR223-lamin A construct was then recombined into the Y2H vectors pAD and/or pDB using LR Clonase. This resulted in five variant panels: 1) pAD-lamin A 2–664 (n = 83 variants), 2) pAD-lamin A 259–664 (n = 59 variants), 3) pDB-lamin A 2–664 (n = 73 variants), 4) pDB-lamin A 259–664 (n = 73 variants), and 5) pDB-Lamin A 388–664 (n = 62 variants). All pAD-lamin A and pDB-lamin A constructs were used to transform haploid yeast strains Y8800 and Y8930, respectively, and are maintained as glycerol stocks.

ACKNOWLEDGMENTS

We thank Song Yi, Sam Pevzner, Ty Voss, and Orna Cohen-Fix for technical expertise. Imaging was performed in the National Cancer Institute High-Throughput Imaging Facility. This work was in part supported by the Intramural Research Program of the National Institutes of Health, National Cancer Institute, Center for Cancer Research, the Progeria Research Foundation, and National Institutes of Health grants HG001715 and HG006066.

REFERENCES

Anderson DJ, Hetzer MW (2008). Reshaping of the endoplasmic reticulum limits the rate for nuclear envelope formation. J Cell Biol 182, 911–924.

Barrowman J, Hamblet C, George CM, Michaelis S (2008). Analysis of prelamin A biogenesis reveals the nucleus to be a CaaX processing compartment. Mol Biol Cell 19, 5398–5408.

Benedetti S *et al.* (2007). Phenotypic clustering of lamin A/C mutations in neuromuscular patients. Neurology 69, 1285–1292.

Bonaldo MF, Lennon G, Soares MB (1996). Normalization and subtraction: two approaches to facilitate gene discovery. Genome Res 6, 791–806.

Bonne G *et al.* (2000). Clinical and molecular genetic spectrum of autosomal dominant Emery-Dreifuss muscular dystrophy due to mutations of the lamin A/C gene. Ann Neurol 48, 170–180.

Bruston F, Delbarre E, Ostlund C, Worman HJ, Buendia B, Duband-Goulet I (2010). Loss of a DNA binding site within the tail of prelamin A contributes to altered heterochromatin anchorage by progerin. FEBS Lett 584, 2999–3004.
Capell BC, Erdos MR, Madigan JP, Fiordalisi JJ, Varga R, Conneely KN, Gordon LB, Der CJ, Cox AD, Collins FS (2005). Inhibiting farnesylation of progerin prevents the characteristic nuclear blebbing of Hutchinson-Gilford progeria syndrome. Proc Natl Acad Sci USA 102, 12879–12884.
Charloteaux B, Zhong Q, Dreze M, Cusick ME, Hill DE, Vidal M (2011). Protein-protein interactions and networks: forward and reverse edgetics. Methods Mol Biol 759, 197–213.
Corrigan DP, Kuszczak D, Rusinol AE, Thewke DP, Hrycyna CA, Michaelis S, Sinensky MS (2005). Prelamin A endoproteolytic processing in vitro by recombinant Zmpste24. Biochem J 387, 129–138.
Crisp M, Liu Q, Roux K, Rattner JB, Shanahan C, Burke B, Stahl PD, Hodzic D (2006). Coupling of the nucleus and cytoplasm: role of the LINC complex. J Cell Biol 172, 41–53.
Dahl KN, Scaffidi P, Islam MF, Yodh AG, Wilson KL, Misteli T (2006). Distinct structural and mechanical properties of the nuclear lamina in Hutchinson-Gilford progeria syndrome. Proc Natl Acad Sci USA 103, 10271–10276.
Dhe-Paganon S, Werner ED, Chi YI, Shoelson SE (2002). Structure of the globular tail of nuclear lamin. J Biol Chem 277, 17381–17384.
Dittmer TA, Misteli T (2011). The lamin protein family. Genome Biol 12, 222.
Dorner D, Gotzmann J, Foisner R (2007). Nucleoplasmic lamins and their interaction partners, LAP2alpha, Rb, and BAF, in transcriptional regulation. FEBS J 274, 1362–1373.
Dreze M, Monachello D, Lurin C, Cusick ME, Hill DE, Vidal M, Braun P (2010). High-quality binary interactome mapping. Methods Enzymol 470, 281–315.
Eriksson M *et al*. (2003). Recurrent de novo point mutations in lamin A cause Hutchinson-Gilford progeria syndrome. Nature 423, 293–298.
Fisher DZ, Chaudhary N, Blobel G (1986). cDNA sequencing of nuclear lamins A and C reveals primary and secondary structural homology to intermediate filament proteins. Proc Natl Acad Sci USA 83, 6450–6454.
Galiova G, Bartova E, Raska I, Krejci J, Kozubek S (2008). Chromatin changes induced by lamin A/C deficiency and the histone deacetylase inhibitor trichostatin A. Eur J Cell Biol 87, 291–303.
Garg A, Subramanyam L, Agarwal AK, Simha V, Levine B, D'Apice MR, Novelli G, Crow Y (2009). Atypical progeroid syndrome due to heterozygous missense LMNA mutations. J Clinic Endocrinol Metab 94, 4971–4983.
Glynn MW, Glover TW (2005). Incomplete processing of mutant lamin A in Hutchinson-Gilford progeria leads to nuclear abnormalities, which are reversed by farnesyltransferase inhibition. Hum Mol Genet 14, 2959–2969.
Goldman RD *et al*. (2004). Accumulation of mutant lamin A causes progressive changes in nuclear architecture in Hutchinson-Gilford progeria syndrome. Proc Natl Acad Sci USA 101, 8963–8968.
Gonzalez JM, Navarro-Puche A, Casar B, Crespo P, Andres V (2008). Fast regulation of AP-1 activity through interaction of lamin A/C, ERK1/2, and c-Fos at the nuclear envelope. J Cell Biol 183, 653–666.
Gonzalez JM, Pla D, Perez-Sala D, Andres V (2011). A-type lamins and Hutchinson-Gilford progeria syndrome: pathogenesis and therapy. Front Biosci 3, 1133–1146.
Gunteski-Hamblin AM, Song G, Walsh RA, Frenzke M, Boivin GP, Dorn GW 2nd, Kaetzel MA, Horseman ND, Dedman JR (1996). Annexin VI overexpression targeted to heart alters cardiomyocyte function in transgenic mice. Am J Physiol 270, H1091–1100.
Hozak P, Sasseville AM, Raymond Y, Cook PR (1995). Lamin proteins form an internal nucleoskeleton as well as a peripheral lamina in human cells. J Cell Sci 108, 635–644.
Huang da W, Sherman BT, Lempicki RA (2009). Systematic and integrative analysis of large gene lists using DAVID bioinformatics resources. Nat Protoc 4, 44–57.
Ivorra C, Kubicek M, Gonzalez JM, Sanz-Gonzalez SM, Alvarez-Barrientos A, O'Connor JE, Burke B, Andres V (2006). A mechanism of AP-1 suppression through interaction of c-Fos with lamin A/C. Genes Dev 20, 307–320.
Jans SW, de Jong YF, Reutelingsperger CP, van der Vusse GJ, van Bilsen M (1998). Differential expression and localization of annexin V in cardiac myocytes during growth and hypertrophy. Mol Cell Biochem 178, 229–236.
Korfali N *et al*. (2012). The nuclear envelope proteome differs notably between tissues. Nucleus 3, 552–564.
Krimm I, Ostlund C, Gilquin B, Couprie J, Hossenlopp P, Mornon JP, Bonne G, Courvalin JC, Worman HJ, Zinn-Justin S (2002). The Ig-like structure of the C-terminal domain of lamin A/C, mutated in muscular dystrophies, cardiomyopathy, and partial lipodystrophy. Structure 10, 811–823.
Kubben N, Voncken JW, Demmers J, Calis C, van Almen G, Pinto Y, Misteli T (2010). Identification of differential protein interactors of lamin A and progerin. Nucleus 1, 513–525.
Kumaran RI, Muralikrishna B, Parnaik VK (2002). Lamin A/C speckles mediate spatial organization of splicing factor compartments and RNA polymerase II transcription. J Cell Biol 159, 783–793.
Lamesch P *et al*. (2007). hORFeome v3.1: a resource of human open reading frames representing over 10,000 human genes. Genomics 89, 307–315.
Lee DC, Welton KL, Smith ED, Kennedy BK (2009). A-type nuclear lamins act as transcriptional repressors when targeted to promoters. Exp Cell Res 315, 996–1007.
Liu B *et al*. (2005). Genomic instability in laminopathy-based premature aging. Nat Med 11, 780–785.
Macara IG (2001). Transport into and out of the nucleus. Microbiol Mol Biol Rev 65, 570–594.
Maier RH, Maier CJ, Onder K (2011). Construction of improved yeast two-hybrid libraries. Methods Mol Biol 729, 71–84.
Manju K, Muralikrishna B, Parnaik VK (2006). Expression of disease-causing lamin A mutants impairs the formation of DNA repair foci. J Cell Sci 119, 2704–2714.
Montes de Oca R, Shoemaker CJ, Gucek M, Cole RN, Wilson KL (2009). Barrier-to-autointegration factor proteome reveals chromatin-regulatory partners. PLoS One 4, e7050.
Muchir A, Bonne G, van der Kooi AJ, van Meegen M, Baas F, Bolhuis PA, de Visser M, Schwartz K (2000). Identification of mutations in the gene encoding lamins A/C in autosomal dominant limb girdle muscular dystrophy with atrioventricular conduction disturbances (LGMD1B). Hum Mol Genet 9, 1453–1459.
Nikolova V *et al*. (2004). Defects in nuclear structure and function promote dilated cardiomyopathy in lamin A/C-deficient mice. J Clin Invest 113, 357–369.
Pegoraro G, Kubben N, Wickert U, Gohler H, Hoffmann K, Misteli T (2009). Ageing-related chromatin defects through loss of the NURD complex. Nat Cell Biol 11, 1261–1267.
Pendas AM *et al*. (2002). Defective prelamin A processing and muscular and adipocyte alterations in Zmpste24 metalloproteinase-deficient mice. Nat Genet 31, 94–99.
Raffaele Di Barletta M *et al*. (2000). Different mutations in the LMNA gene cause autosomal dominant and autosomal recessive Emery-Dreifuss muscular dystrophy. Am J Hum Genet 66, 1407–1412.
Rankin J, Ellard S (2006). The laminopathies: a clinical review. Clin Genet 70, 261–274.
Reichart B, Klafke R, Dreger C, Kruger E, Motsch I, Ewald A, Schafer J, Reichmann H, Muller CR, Dabauvalle MC (2004). Expression and localization of nuclear proteins in autosomal-dominant Emery-Dreifuss muscular dystrophy with LMNA R377H mutation. BMC Cell Biol 5, 12.
Rober RA, Weber K, Osborn M (1989). Differential timing of nuclear lamin A/C expression in the various organs of the mouse embryo and the young animal: a developmental study. Development 105, 365–378.
Saj M, Dabrowski R, Labib S, Jankowska A, Szperl M, Broda G, Szwed H, Tesson F, Bilinska ZT, Ploski R (2012). Variants of the lamin A/C (LMNA) gene in non-valvular atrial fibrillation patients: a possible pathogenic role of the Thr528Met mutation. Mol Diagn Ther 16, 99–107.
Savage DB *et al*. (2004). Familial partial lipodystrophy associated with compound heterozygosity for novel mutations in the LMNA gene. Diabetologia 47, 753–756.
Scharner J *et al*. (2011). Novel LMNA mutations in patients with Emery-Dreifuss muscular dystrophy and functional characterization of four LMNA mutations. Hum Mutat 32, 152–167.
Schirmer EC, Gerace L (2005). The nuclear membrane proteome: extending the envelope. Trends Biochem Sci 30, 551–558.
Sebillon P *et al*. (2003). Expanding the phenotype of LMNA mutations in dilated cardiomyopathy and functional consequences of these mutations. J Med Genet 40, 560–567.
Shumaker DK, Solimando L, Sengupta K, Shimi T, Adam SA, Grunwald A, Strelkov SV, Aebi U, Cardoso MC, Goldman RD (2008). The highly

conserved nuclear lamin Ig-fold binds to PCNA: its role in DNA replication. J Cell Biol 181, 269–280.
Skrahina T, Piljic A, Schultz C (2008). Heterogeneity and timing of translocation and membrane-mediated assembly of different annexins. Exp Cell Res 314, 1039–1047.
Spann TP, Goldman AE, Wang C, Huang S, Goldman RD (2002). Alteration of nuclear lamin organization inhibits RNA polymerase II-dependent transcription. J Cell Biol 156, 603–608.
Stuurman N, Heins S, Aebi U (1998). Nuclear lamins: their structure, assembly, and interactions. J Struct Biol 122, 42–66.
Sullivan T, Escalante-Alcalde D, Bhatt H, Anver M, Bhat N, Nagashima K, Stewart CL, Burke B (1999). Loss of A-type lamin expression compromises nuclear envelope integrity leading to muscular dystrophy. J Cell Biol 147, 913–920.
Suzuki Y, Kagawa N, Fujino T, Sumiya T, Andoh T, Ishikawa K, Kimura R, Kemmochi K, Ohta T, Tanaka S (2005). A novel high-throughput (HTP) cloning strategy for site-directed designed chimeragenesis and mutation using the Gateway cloning system. Nucleic Acids Res 33, e109.
Szeverenyi I *et al*. (2008). The Human Intermediate Filament Database: comprehensive information on a gene family involved in many human diseases. Hum Mutat 29, 351–360.
Taniura H, Glass C, Gerace L (1995). A chromatin binding site in the tail domain of nuclear lamins that interacts with core histones. J Cell Biol 131, 33–44.
Verstraeten VL *et al*. (2006). Compound heterozygosity for mutations in LMNA causes a progeria syndrome without prelamin A accumulation. Hum Mol Genet 15, 2509–2522.
Vytopil M *et al*. (2003). Mutation analysis of the lamin A/C gene (LMNA) among patients with different cardiomuscular phenotypes. J Med Genet 40, e132.
Weber K, Plessmann U, Traub P (1989). Maturation of nuclear lamin A involves a specific carboxy-terminal trimming, which removes the polyisoprenylation site from the precursor; implications for the structure of the nuclear lamina. FEBS Lett 257, 411–414.
Worman HJ, Bonne G (2007). "Laminopathies": a wide spectrum of human diseases. Exp Cell Res 313, 2121–2133.
Yamamoto Y, Yoshida A, Miyazaki N, Iwasaki K, Sakisaka T (2014). Arl6IP1 has the potency to shape the mammalian ER membrane in a reticulon-like fashion. Biochem J 458, 69–79.
Yang YS, Strittmatter SM (2007). The reticulons: a family of proteins with diverse functions. Genome Biol 8, 234.
Ye Q, Worman HJ (1995). Protein-protein interactions between human nuclear lamins expressed in yeast. Exp Cell Res 219, 292–298.
Yuan JH, Hu J, Zhao Z, Shen HR, Li N, Bing Q (2010). Mutation analysis of a Chinese family with autosomal dominant Emery-Dreifuss muscular dystrophy [in Chinese]. Chin J Med Genet 27, 136–139.
Zastrow MS, Vlcek S, Wilson KL (2004). Proteins that bind A-type lamins: integrating isolated clues. J Cell Sci 117, 979–987.